Eur Biophys J (1990) 18:175–191

European Biophysics Journal

Coupling of proton flow and rotation in the bacterial flagellar motor: stochastic simulation of a microscopic model

B. Kleutsch and P. Läuger

Fakultät für Biologie der Universität, Universitätsstrasse 10, D-7750 Konstanz, Federal Republic of Germany

Received October 8, 1989/Accepted in revised form December 18, 1989

Summary. The rotatory motor of bacterial flagella is driven by a transmembrane electrochemical gradient of protons. A model of the flagellar motor is analysed, which is based on the notion that protons passing through the motor use a channel-like pathway formed by ligand groups located partly on the rotor, partly on the stator. Proton translocation is linked to the displacement of stator elements which are elastically bound to the cell wall. The model is described by a cyclic sequence of translocation steps and proton binding and release reactions. Stochastic simulations of the model are carried out in which transitions between the states of the reaction cycle are treated as random events. In this way the rotation frequency can be predicted as a function of experimental variables such as driving force and viscous load. Furthermore, the effects of microscopic parameters such as the transition frequencies of stator elements and the force constant of elastic coupling on the dynamic properties of the motor can be studied. The model allows for intrinsic uncoupling ("slippage") resulting from translocation steps without associated rotational movement. It is shown that mechanistic information can be obtained by studying random fluctuations of rotational speed.

Key words: Flagellar motor – Bacterial locomotion – Proton channel – Protonmotive force – Force generation

Introduction

The bacterial flagellar motor is a device that couples transmembrane ion flow to rotary motion (Berg 1975; Silverman and Simon 1977; Macnab 1978; Silverman 1980; Berg et al. 1982; Macnab and Aizawa 1984; Macnab 1987; Stewart and Dahlquist 1987; Khan 1988). The force driving the rotation of the flagellum is generated in the basal body which is embedded in the cell wall and the plasma membrane. The basal body of gram-positive bacteria contains two parallel rings of 20–30 nm diameter. The *M* ring is coplanar with the plasma membrane and is assumed to be rigidly attached to the flagellum. The *S* ring is located on the external side of the membrane and is likely to be connected with the cell wall. Gram-negative bacteria such as *Escherichia coli* have two additional rings which are associated with the peptidoglycane layer and the outer lipopolysaccharide membrane; they probably serve as bearings and do not participate in force generation.

The flagellar motor contains several quasi-independent force-generating units. Evidence for this notion comes from experiments with paralysed *mot* mutants of *E. coli* in which induction of the synthesis of *mot A* and *mot B* proteins leads to a stepwise increase of rotation speed (Block and Berg 1984; Blair and Berg 1988). From the size of the speed increment the existence of 16 (Block and Berg 1984) or 8 (Blair and Berg 1988) independent units has been inferred. These findings may be compared with results of electron microscopic studies which gave evidence for 16-fold rotational symmetry in the *M* ring (De Pamphilis and Adler 1971). In freeze-fracture electron micrographs of the gram-negative bacterium Aquaspirillum serpens, a similar number (14–16) of membrane particles ("studs") is seen at the periphery of annular depressions, normally occupied by one of the rings (Coulton and Murray 1978). Comparable results were recently obtained in freeze-fracture studies of *Streptococcus* and *E. coli* (Khan et al. 1988). It is feasible, as Blair and Berg (1988) proposed, that two particles are present per force generator. The *mot* proteins are not found in preparations of isolated basal bodies but remain with the cytoplasmic membrane (Ridgeway et al. 1977).

In *E. coli* and in a number of other bacteria the motor is driven by a transmembrane electrochemical gradient of H^+ (Belyakova et al. 1976; Manson et al. 1977; Matsuura et al. 1977; Khan and Macnab 1980; Ravid and Eisenbach 1984). In alkalophilic bacteria the driving ion seems to be Na^+ (Krulwich 1986). It has been estimated that at a driving force of 100–200 mV, the passage of a few hundred protons per revolution is sufficient to sustain rota-

Offprint requests to: P. Läuger

tion of the motor at high viscous load (Berg 1974). More recently, from flux measurements the number of protons passing through the motor in one revolution has been determined to be ~1200 (Meister et al. 1987). When the load is heavy, the motor operates at constant torque, the rotation rate being inversely proportional to the viscosity of the medium (Berg and Turner 1979; Manson et al. 1980). When the load is light, the motor runs at a constant limiting rate, independent of the load (Lowe et al. 1987). The motor can switch from clockwise to counterclockwise rotation and it can be driven artificially by a proton-motive force of reverse polarity (Manson et al. 1980).

Several models for the coupling beween ion flow and flagellar rotation have been proposed so far (Läuger 1977; Glagolev and Skulachev 1978; Macnab 1980; Oosawa and Masai 1982; Berg and Khan 1983; Läuger 1988; Kobayashi 1988; Meister et al. 1989; Murata et al. 1989). In a previous study (Läuger 1988) a mechanism has been described in which the ion passing through the motor interacts simultaneously with ligand groups located on the *M* ring (the "rotor") and ligand groups located on "stator" elements attached to the cell wall. From an approximate treatment of the model, predictions on the relationship between torque and rotation rate have been derived. For this purpose, a number of simplifying assumptions had to be introduced. In particular, the analysis had to be restricted to high ion concentrations at which the binding sites are mostly occupied. In the following, we carry out a more general analysis based on a computer simulation of the model. Using a random-number method, the stochastic nature of ion permeation and force generation can be taken explicitely into account. In this way the dependence of dynamic properties of the motor on microscopic parameters of the model can be studied.

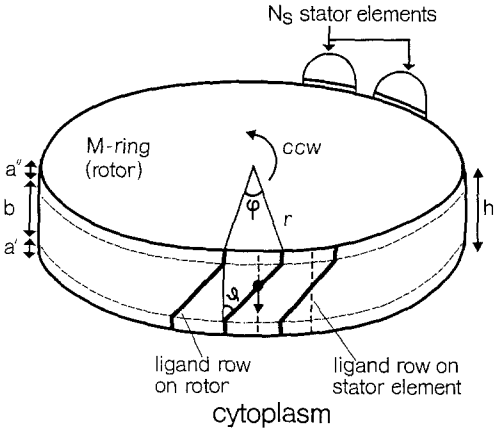

Fig. 1. Arrangement of ligand rows (half-channels) on rotor (*M* ring) and stator. The central part of the rotor half-channel is oriented at an angle ϑ with respect to the half-channel on the stator element. Inward movement of an ion occupying the intersection site leads to counterclockwise (ccw) rotation of the rotor. The dashed lines indicate the location of the entrance sites of the proton channel. Protons are assumed to move freely from the aqueous medium to the entrance sites through access channels (axially-oriented parts of the rotor half-channel)

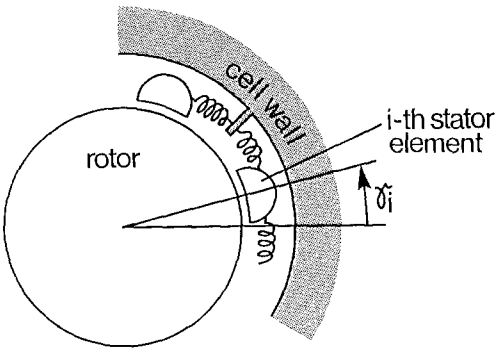

Fig. 2. The stator elements are assumed to be elastically coupled to the cell wall. γ_i is the deflection angle of the *i*-th stator element with respect to its resting position relative to the cell wall

Microscopic model of the flagellar motor

The model is based on the notion that the ion pathway through the motor represents a kind of "channel" consisting of a series of polar ligand groups with which the ion interacts in an energetically favourable way (Läuger 1977; Macnab 1979). We assume that the *M* ring is surrounded by a number of "stator elements" attached to the cell wall, each containing a ligand row perpendicular to the plane of the ring (Fig. 1). The *mot A* and/or *mot B* gene products may be identical with, or part of, these stator elements. At the periphery of the *M* ring ligand rows are assumed to be present that are oriented at an angle ϑ with respect to the ligand rows on the stator elements (Fig. 1). We further assume that the energy of interaction of the ion with a single ligand row is not sufficient to compensate for the energy required to remove the ion from water, but that an energetically favourable situation results when the ion is located at the site of intersection of the two ligand rows where it has about twice as many ligand groups available. Under these conditions the ion is constrained to move together with the intersection point. For the geometrical arrangement depicted in Fig. 1, ion flow from the external medium to the cytoplasm leads to counterclockwise rotation of the *M* ring. ("Clockwise" and "counterclockwise" refer to the direction of rotation as seen from the extracellular side.) As shown in Fig. 1, the oblique ligand-rows (or half channels) on the circumference of the rotor are assumed to be narrowly spaced without overlap. Their number N_r is then given by

$$N_r = \frac{2\pi}{\varphi} \tag{1}$$

where φ is the angle subtended by a half-channel.

Following Berg and Khan (1983) we assume that the stator elements are elastically coupled to the cell wall so that they can carry out restricted motion along the circumference of the *M* ring (Fig. 2). When a stator element moves while the rotor retains its position, elastic energy is stored which may be released in a subsequent rotation of the ring. In this way each stator element may act as a (quasi-) independent force generator.

If γ_i is the angle of deflection of the *i*-th stator element S_i with respect to its resting position relative to the cell

wall and q the force constant of elastic coupling of a stator element to the cell wall, the restoring torque M_i acting on S_i is given by

$$M_i = -q\gamma_i \tag{2}$$

where γ_i is taken to be positive when S_i is deflected in a counterclockwise direction; accordingly, a torque $M_i > 0$ tends to rotate the M ring in a counterclockwise direction. Implicit in (2) is the assumption that the stator elements are independent of each other. The mean torque M exerted by the stator elements on the rotor is then obtained as

$$M = \sum_i \langle M_i \rangle = -q N_s \langle \gamma \rangle \tag{3}$$

where N_s is the total number of stator elements and $\langle \gamma \rangle$ is the time average of the deflection angle.

Reaction cycle

We assume that the relative motion of the stator element S with respect to the M ring occurs in discrete steps. The motion of S may then be described by a potential profile consisting of a series of potential wells separated by activation barriers (Fig. 3). The entrance sites of the channel (0 and $n+1$) are assumed to be connected with the aqueous phase by "access channels" of length a' and a'' (Fig. 1) in which the protons are able to move freely. For simplicity, we assume that the location of the barriers and wells is the same, irrespective of whether the intersection site is empty or occupied. Accordingly, motion of the stator element and ion translocation is described by the reaction scheme of Fig. 4. Empty states of the intersection site are denoted by A and occupied states by B; A_j and B_j are states in which the intersection site is located at the position of the j-th energy well (Fig. 3).

When the motor performs clockwise rotation, the cycle may start in state A_0 by binding H^+ from the cytoplasm ($A_0 \rightarrow B_0$). The system may then move through $B_1, B_2, \ldots, B_n$ to B_{n+1}. After release of the proton to the external side ($B_{n+1} \rightarrow A_{n+1}$), a transition to state A_0'' can take place in which the next ligand row on the rotor intersects with the ligand row on the stator in position 0. (Under physiological conditions, i.e., for an inward-directed proton gradient, the sequence of events is the inverse.)

At non-saturating proton concentration, cycles with empty binding site ($A_0 \rightarrow A_1 \rightarrow \ldots \rightarrow A_{n+1}$) will occasionally occur. This represents a loss of strict coupling between proton flux and rotational motion. At low driving force, the system carries out a biased random walk among the states of the reaction cycle, corresponding to a superposition of steady rotation and Brownian motion.

Equilibrium reactions

For the analysis of the reaction scheme of Fig. 4 we introduce the probability $x[Y]$ that the stator half-channel is

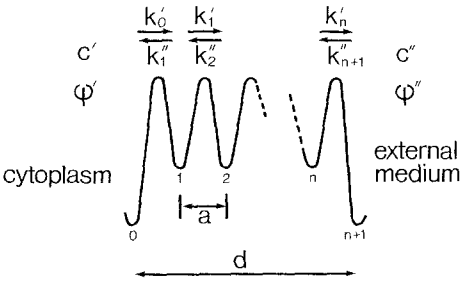

Fig. 3. Potential-energy profile describing the relative motion of the stator element with respect to the rotor. $d = b/\cos\vartheta$ is the length of the central part of the rotor half-channel (Fig. 1) and a the distance between neighbouring energy wells. c' and c'' are the proton concentrations on the cytoplasmic and extracellular side of the M ring, respectively; ψ' and ψ'' are the electric potentials. Rate constants for crossing the barriers are denoted by k'_j, k''_j (intersection site empty) and by l'_j, l''_j (intersection site occupied). The entrance sites (0 and $n+1$) of the channel are connected with the aqueous media by access channels of length a' and a'' (Fig. 1) in which protons are able to diffuse freely

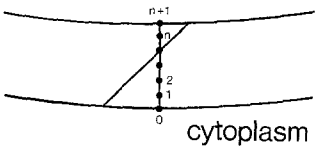

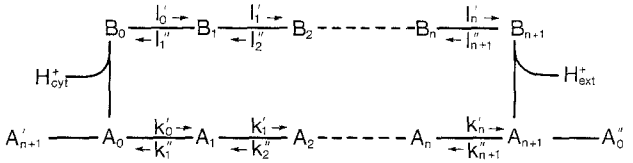

Fig. 4. Relative motion of the stator element with respect to the rotor (M ring), represented as a sequence of transitions between discrete states. States with empty intersection site are denoted by A, states with occupied intersection by B. A_j and B_j are states in which the intersection site is located at the j-th potential well (Fig. 3). k'_j, k''_j, l'_j and l''_j are rate constants

in state Y:

$$\sum_{j=0}^{n+1} \{x[A_j] + x[B_j]\} = 1. \tag{4}$$

Assuming that protonation and deprotonation of the entrance sites ($j=0$ and $j=n+1$) are not rate-limiting, the probability of states A_0, B_0, A_{n+1} and B_{n+1} can be expressed by equilibrium dissociation constants K' and K'':

$$\frac{x[B_0]}{x[A_0]} = \frac{c'}{K'}; \qquad \frac{x[B_{n+1}]}{x[A_{n+1}]} = \frac{c''}{K''} \tag{5}$$

where c' and c'' are the proton concentrations in the cytoplasmic and in the extracellular medium, respectively.

The assumption that binding and release of protons are equilibrium reactions is likely to be fulfilled under most conditions. The apparent bimolecular rate constant for protonation of a proton-accepting site in an ion channel may be as high as $4 \cdot 10^{11}\ M^{-1}\ s^{-1}$ (Prod'hom et al. 1987). At $pH \approx pK \approx 7$ this yields protonation and depro-

tonation rates of about $4 \cdot 10^4\ s^{-1}$. On the other hand, the average proton translocation rate through a single stator element is equal to $v N_r$, where v is the rotation rate and N_r the number of half-channels on the rotor. With $v = 200\ s^{-1}$ and $N_r = 20$, the translocation rate becomes $4000\ s^{-1}$, about ten times smaller than the estimated protonation/deprotonation rate. Still higher rates of protonation and deprotonation may be estimated when buffering is taken into account (Appendix A).

When the system is in state A_{n+1}, the rotor half-channel intersects with the external entrance site of the stator half-channel (Fig. 4). A transition may then occur to state A_0'' in which the next rotor half-channel intersects with the cytoplasmic entrance site of the stator half-channel; as indicated by Fig. 1, this transition may occur with negligible shift in the angular position of the rotor. Assuming that the energy barrier between states A_{n+1} and A_0'' is low, these states are always in equilibrium with each other:

$$\frac{x[A_{n+1}]}{x[A_0]} = H. \tag{6}$$

(In this relation A_0 is written instead of A_0'', since all rotor half-channels can be assumed to have identical properties). The quantity H is a voltage-independent equilibrium constant which may be set equal to unity.

Dependence of kinetic parameters on voltage and elastic restoring forces

For generality, we assume that part of the transmembrane voltage drops across access channels oriented parallel to the rotor axis, which connect the entrance sites to the aqueous phases (Fig. 1). Under this condition the entrance sites act as "ion wells" (Mitchell and Moyle 1974), i.e., the equilibrium dissociation constants K' and K'' of H^+ become functions of voltage. The lengths of the access channels are denoted by a' and a'' and the total length over which the voltage drops by h (Fig. 1). If $\alpha' = a'/h$ and $\alpha'' = a''/h$ are the fractions of total voltage $\psi' - \psi''$ across the access channels at the inner (cytopasmic) and the outer (extracellular) side, respectively, the proton dissociation constants are given by

$$K' = \tilde{K}' \exp(-\alpha' u) \tag{7}$$

$$K'' = \tilde{K}'' \exp(\alpha'' u) \tag{8}$$

$$u \equiv \frac{\psi' - \psi''}{k T/e_0} = \frac{\Delta\psi}{k T/e_0} \tag{9}$$

where $\tilde{K}'$ and $\tilde{K}''$ are the values of K' and K'' at zero voltage. k is Boltzmann's constant, T the absolute temperature and e_0 the charge of the proton. The representation of α' and α'' by geometrical distances (a'/h and a''/h) is only approximately valid. More generally, α' and α'' have to be considered as relative dielectric distances depending on the dielectric properties of the rotor/stator system.

The rate constants k_j', k_j'', l_j' and l_j'' for transitions of stator elements between adjacent energy wells are determined by the height of the activation barriers. In the following we assume that the barriers are symmetric and that the energy wells are regularly spaced; the distance between adjacent wells in Fig. 3 then becomes $a = d/(n+1)$, where d is the length of the oblique part of the rotor half-channel (Figs. 1 and 3). If the stator element is moved from a well to the top of the adjacent barrier, the deflection angle γ changes by $\Delta\gamma = \varphi/2(n+1)$. This corresponds to an energy change ΔE due to elastic restoring forces:

$$\Delta E = q \int_{\gamma}^{\gamma+\Delta\gamma} \gamma \, d\gamma = q \, \Delta\gamma(\gamma + \Delta\gamma/2). \tag{10}$$

(Note that the deflection angle γ can vary independently of the relative position of the stator element with respect to the rotor). According to the theory of absolute reaction rates (Zwolinsky et al. 1949), the rate constant for jumps from j to $j+1$ becomes $k_j' = \tilde{k}_j' \exp(-\Delta E/k T)$ where $\tilde{k}_j'$ is the value of k_j for $\Delta E = 0$. With $\Delta\gamma = \varphi/2(n+1) = \pi/N_r(n+1)$ this yields:

$$k_j' = \tilde{k}_j' \exp\left[-\frac{s(\gamma + y)}{n+1}\right] \tag{11}$$

$$k_j'' = \tilde{k}_j'' \exp\left[\frac{s(\gamma - y)}{n+1}\right] \tag{12}$$

$$s \equiv \frac{\pi q}{k T N_r}; \qquad y \equiv \frac{\pi}{2 N_r(n+1)}. \tag{13}$$

If a proton is located in the intersection site, an additional electrostatic term $-e_0(\psi' - \psi'')\, b/2h(n+1)$ is added to the energy change ΔE (10); e_0 is the charge of the proton, b the axial distance between the entrance sites (Fig. 1), and ψ' and ψ'' are the electric potentials at the cytoplasmic and extracellular side, respectively. This yields for the rate constants of transitions with occupied intersection site:

$$l_j' = \tilde{l}_j' \exp\left[-\frac{s(\gamma + y) - \beta u/2}{n+1}\right] \tag{14}$$

$$l_j'' = \tilde{l}_j'' \exp\left[\frac{s(\gamma - y) - \beta u/2}{n+1}\right] \tag{15}$$

$$\beta = \frac{b}{h} = 1 - \alpha' - \alpha''. \tag{16}$$

$\tilde{l}_j'$ and $\tilde{l}_j''$ are the values of l_j' and l_j'' in the absence of elastic and electrostatic forces. According to the principle of detailed balance, the rate constants and equilibrum constants are not independent of each other, but connected by the relations

$$\frac{\tilde{k}_0' \, \tilde{k}_1' \ldots \tilde{k}_n'}{\tilde{k}_1'' \, \tilde{k}_2'' \ldots \tilde{k}_{n+1}''} = H \tag{17}$$

$$\frac{\tilde{l}_0' \, \tilde{l}_1' \ldots \tilde{l}_n'}{\tilde{l}_1'' \, \tilde{l}_2'' \ldots \tilde{l}_{n+1}''} = \frac{\tilde{K}' H}{\tilde{K}''}. \tag{18}$$

For a derivation of (17) and (18), see Appendix B.

Transition probabilities

The numerical simulations to be described below are based on the probabilities $\Delta P = r(Y)\,\Delta t$ that a stator element which is in state $Y \in (A_j, B_j)$ will leave this state within time interval Δt. For the "inner" states $A_1, \ldots, A_n, B_1, \ldots, B_n$, the transition frequencies are given by

$$r(A_j) = k'_j + k''_j \tag{19}$$

$$r(B_j) = l'_j + l''_j \qquad (i = 1, 2, \ldots, n). \tag{20}$$

Since the "outer" states A_0, B_0, A_{n+1} and B_{n+1} have been assumed to be in equilibrium with each other, they may be combined into a compound state C. The conditional probabilities $P(Y|C) \equiv p(Y)$ that a stator element is in a particular state $Y \in (A_0, B_0, A_{n+1}, B_{n+1})$, given that it is in the compound state C, are obtained from (5) and (6):

$$p(A_0) = \sigma; \qquad p(A_{n+1}) = H\sigma \tag{21}$$

$$p(B_0) = \sigma c'/K'; \qquad p(B_{n+1}) = H\sigma c''/K'' \tag{22}$$

$$1/\sigma \equiv 1 + c'/K' + H(1 + c''/K'')\,. \tag{23}$$

Accordingly, the frequency of transitions out of state C is given by:

$$r(C) = p(A_0)\,k'_0 + p(B_0)\,l'_0 + p(A_{n+1})\,k''_{n+1} + p(B_{n+1})\,l''_{n+1}\,. \tag{24}$$

Rotational relaxation

Superimposed on the discrete, stepwise motion of the stator elements is the continuous rotation of the M ring under the influence of elastic restoring forces. For generality, we allow for the possibility that, in addition to the torque M generated by the motor, an externally applied torque M_e acts on the flagellum (Meister et al. 1989; Block et al. 1989). Since inertial forces are negligible [1], the total torque $M + M_e$ is exactly cancelled by the torque $-f \cdot \omega$ arising from frictional forces (f is the friction coefficient and ω the angular speed):

$$M + M_e = f\,\omega \tag{25}$$

where ω is taken to be positive for counterclockwise rotation. Rotation of the M ring, which is described by a rotation angle ϱ, results in a synchronous change of the deflection angles γ_i of the stator elements:

$$\omega = \frac{\mathrm{d}\varrho}{\mathrm{d}t} = \frac{\mathrm{d}\gamma_i}{\mathrm{d}t} \qquad (i = 1, 2, \ldots, N_s) \tag{26}$$

[1] From the geometry of the flagellum, an upper limit of its moment of inertia may be estimated to be $I < 4 \cdot 10^{-29}\ \mathrm{Js}^2$. With a friction coefficient of the flagellum of $f \approx 4 \cdot 10^{-21}$ Js (Lowe et al. 1987), the ratio of the kinetic energy of rotation divided by the energy per revolution dissipated by friction becomes $I\,\nu/2\,f \approx 5 \cdot 10^{-7}$ ($\nu \approx 100$ Hz is the rotation rate). This means that the motion of the flagellum is totally dominated by friction

Equations (2), (3), (25) and (26) together yield:

$$M = \sum_j M_j$$

$$f\,\frac{\mathrm{d}\gamma_i}{\mathrm{d}t} = -q \sum_j \gamma_j + M_e\,. \tag{27}$$

This equation has the solution

$$\gamma_i(t) - \gamma_i(0) = \varrho(t) - \varrho(0) = \varrho^*\,[1 - \exp(-t/\tau_r)] \tag{28}$$

$$\varrho^* \equiv \frac{1}{N_s}\left[\frac{M_e}{q} - \sum_j \gamma_j(0)\right] \tag{29}$$

$$\tau_r \equiv f/N_s\,q\,. \tag{30}$$

Thus, in the time intervals between jumps of stator elements, the angles γ_i and ϱ exhibit an exponential relaxation behaviour described by a time constant $\tau_r = f/N_s\,q$.

Stochastic simulations

In the model described above, the individual stator elements interact with each other in a complicated manner via rotational motions of the M ring. For this reason an analytical solution for the average rotation speed v is difficult to obtain. Predictions on the dependence of v on experimental variables such as driving force or viscous load can be derived, however, by simulating the stochastic behaviour of the system on a digital computer. Two different methods have been used for this purpose.

Method A

At time $t = 0$, an arbitrary initial state (A_j, B_j) is assigned to the individual stator elements S_i, and initial values of the displacement angles γ_i are chosen at random. With these values of γ_i, the probability $\Delta P_i = r_i(Y)\,\Delta t$ that a transition occurs within Δt is calculated for each S_i, using (19), (20) and (24). The time interval Δt has to be sufficiently short, so that the condition $\Delta P_i \ll 1$ is always met. For each stator element S_i it is decided whether a transition actually occurs within Δt. For this purpose a random number R with a homogeneous distribution in the interval (0, 1) is compared with ΔP_i. R was generated by the algorithm of Kirkpatrick and Stoll (1981). If $R < \Delta P_i$, the stator element is allowed to jump. (This procedure is based on the fact that the probability that a random number $R \in (0, 1)$ is smaller than a given number $Z \in (0, 1)$ is equal to Z). A new random number R is then used to decide to which side the jump takes place. If, for instance, the stator element is in state A_1 before the jump, the probability that the transition is directed from A_1 to A_2 is equal to $k'_1/(k'_1 + k''_1)$. Or, if the stator element is in the compound state C, the probability for a transition into state A_1 is equal to $p(A_0)\,k'_0/r(C)$, and so forth. After this procedure has been completed for all N_s stator elements, the rotor is allowed to rotate under the influence of the elastic restoring forces during the time interval Δt. According to (27), the displacement angles γ_i and the rota-

tion angle ϱ change by $\Delta\gamma_i = \Delta\varrho = \varrho^* [1 - \exp(-\Delta t/\tau_r)]$ during Δt. Thereafter, the whole cycle is repeated for the next time step Δt.

Method B

This method makes explicit use of the distribution of waiting times. The mean waiting time τ_w is defined as the average time the system spends in a given state until a transition occurs in one of the stator elements. τ_w is related to the transition rates $r_i(Y)$ which can be obtained from (19), (20) and (24):

$$\frac{1}{\tau_w} = \sum_{i=1}^{N_s} r_i(Y). \tag{31}$$

The distribution of waiting times t_w which corresponds to a Poisson process is described by a probability density $g(t_w)$:

$$g(t_w) = (1/\tau_w) \exp(-t_w/\tau_w) \tag{32}$$

(Cox and Miller 1977). For a given state of the system, a random waiting time t_w is chosen according to

$$t_w = -\tau_w \ln R \tag{33}$$

where $R \in (0, 1)$ is a random number. This procedure leads to a distribution of waiting times corresponding to (32) (Cox and Miller 1977). In the next step it is decided in which stator element and in which direction the jump occurs. For this purpose the interval (0, 1) is divided into as many subintervals as there exist transition possibilities in the whole system (two for each stator element S_i, if S_i is in one of the states $A_1, \ldots, A_n, B_1, \ldots, B_n$ and four, if S_i is in the compound state C). The length s of each subinterval is determined by the relative frequency of the corresponding transition. For instance, the value of s corresponding to the transition $A_j \rightarrow A_{j+1}$ of stator element S_i is equal to $k'_j \tau_w$. After the assignment of the new state, the rotor is allowed to relax (as in method A), and the cycle is repeated.

Within the limits of statistical error, both methods gave identical results. Method B requires much less computing time, since in method A many time steps Δt are needed for a jump of a stator element. Accordingly, in most cases method B has been used. If not otherwise indicated, the simulations were carried out for $5 \cdot 10^5$ events.

Numerical values of the model parameters

In all simulations, a value of $N_r = 20$ was used for the number of half-channels on the M ring. The number N_s of stator elements was varied between 1 and 20, corresponding to the range (8 or 16) of previous experimental estimates for the maximum number of force-generating units (Block and Berg 1984; Blair and Berg 1988). The number n of energy wells depends on assumptions on the length of the channel and on the geometry of the binding sites (Hille 1984). If the channel length b (Fig. 1) is assumed to be 2–5 nm, the range of n may be estimated to be 4–10. In most simulations a fixed value of $n = 5$ was used; furthermore, in most cases the length of the access channels was set equal to zero ($\alpha' = \alpha'' = 0$).

Experimental data from which the equilibrium dissociation constants $\tilde{K}'$ and $\tilde{K}''$ of H^+ at the entrance sites of the channel can be estimated are not available so far. For simplicity it is assumed that $\tilde{K}' = \tilde{K}'' \equiv K$. A lower limit of K is given by the requirement that the dissociation rate constant k_{off} of H^+ should be larger than the proton translocation rate νN_r through a single stator element. With $\nu N_r \approx 4000\ s^{-1}$ (see above) and an apparent protonation rate constant of $k_{on} \approx 4 \cdot 10^{11}\ M^{-1}\ s^{-1}$ (Prod'hom et al. 1987), a lower limit $K = k_{off}/k_{on} > 10^{-8}$ M is obtained. On the other hand, if K is much larger than physiological proton concentrations ($10^{-8} - 10^{-6}$ M), channel occupancy would be low, which would reduce the efficiency of the motor. In the following, a fixed value $K = 10^{-7}$ M is used.

If not otherwise indicated, all rate constants for jumps of stator elements were taken to be the same in the empty and occupied states of the channel: $\tilde{k}'_j = \tilde{k}''_j \equiv \tilde{k} = \tilde{l}'_j = \tilde{l}''_j \equiv \tilde{l}$. In the simulations, $\tilde{k} = \tilde{l}$ were considered as adjustable parameters which were chosen to fit the experimentally observed rotation frequencies ν. (For an order-of-magnitude estimate, $\tilde{k}$ and $\tilde{l}$ can be set equal to the stepping rate of the motor. With rotation frequencies of $\approx 100\ s^{-1}$ (at a driving force of about 100 mV and low viscous load) and $N_r(n+1)$ steps per revolution, values of $\tilde{k}$ and $\tilde{l}$ of the order of $10^4\ s^{-1}$ may be estimated).

The friction coefficient f can vary over a wide range. In experiments with tethered cells in which friction is determined by the viscous drag experienced by the rotating cell body, f is of the order of $5 \cdot 10^{-20}$ J s, whereas the friction coefficient of a freely rotating flagellum may be as low as $5 \cdot 10^{-22}$ J s (Lowe et al. 1987).

The force constant q of elastic coupling between stator element and cell wall is arbitrarily assigned by the condition $q\,\varphi^2 \approx 10$ kT. When a stator element is displaced from its equilibrium position ($\gamma = 0$) by an angle $\Delta\gamma = \varphi/(n+1)$, corresponding to the distance between adjacent energy wells, the elastic energy increases by $\Delta E = q(\Delta\gamma)^2/2 = q\,\varphi^2/2(n+1)^2$. The condition $q\,\varphi^2 = 10$ kT then means that for small values of n the energy difference ΔE is of the order of kT or lower. Much smaller values of q would lead to unreasonably high thermal displacements, whereas with larger values of q, the stator element would be locked in its equilibrium position. Accordingly, with $\varphi = 2\pi/N_r = 2\pi/20$, the force constant has to be chosen to be $q \approx 4 \cdot 10^{-19}$ J at $T = 298$ K.

With $q = 4 \cdot 10^{-19}$ J, $N_s = 10$ and $f = 5 \cdot 10^{-22}$ J s (corresponding to a freely rotating flagellum), the time constant for rotational relaxation of the M ring is estimated to be $\tau_r = f/N_s q \approx 10^{-4}\ s^{-1}$. Thus, τ_r is of comparable magnitude or larger than the mean dwell time $1/\tilde{k} \approx 1/\tilde{l}$ of the stator element in the energy well, if $\tilde{k}$ and $\tilde{l}$ lie in the range of $5 \cdot 10^3 - 5 \cdot 10^4\ s^{-1}$, as assumed above.

The parameter values which were held fixed in the simulations (if not otherwise indicated) are listed in Table 1.

Table 1. Parameter values which were held fixed in the simulation (if not otherwise indicated)

Parameter	N_r	n	$\tilde{K}'=\tilde{K}''\equiv K$	H	$\alpha'=\alpha''$	$\tilde{k}=\tilde{l}$	q	T
Value	20	5	10^{-7} M	1	0	$2\cdot10^{4}\,s^{-1}$	$4\cdot10^{-19}$ J	298 K

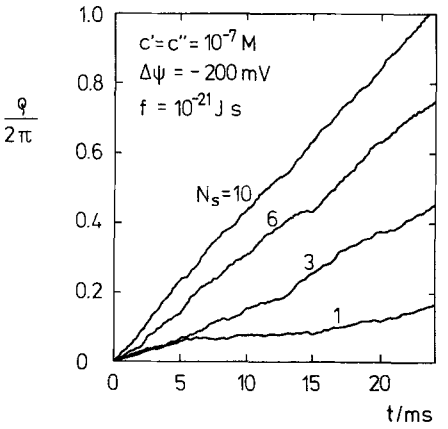

Fig. 5. Rotation angle ϱ of the rotor (in units of 2π) as a function of time t. N_s is the number of stator elements and $\Delta\psi\equiv\psi'-\psi''$ the transmembrane voltage. The simulations were carried out by method A with time steps $\Delta t=0.05/\tilde{k}=2.5$ μs, using the following parameters: $c'=c''=10^{-7}$ M, $f=10^{-21}$ J s; the values of the other parameters are given in Table 1. ϱ was sampled at intervals of 500 μs. The lines were redrawn from the original record

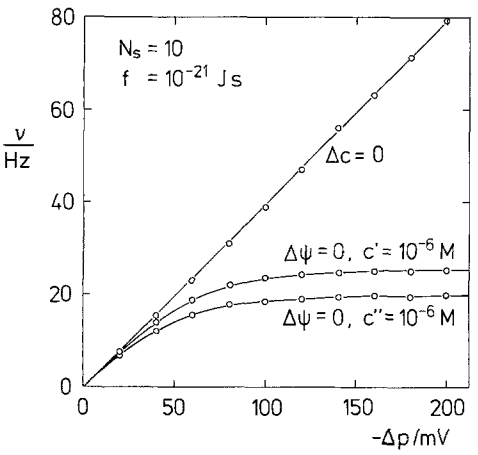

Fig. 6. Rotation frequency ν as a function of driving force Δp. Upper curve: purely electric driving-force ($\Delta p=\Delta\psi$; $c'=c''=10^{-6}$ M). Middle and lower curve: purely osmotic driving-force ($\Delta\psi=0$); c' (middle curve) or c'' (lower curve) were held fixed at 10^{-6} M, and the proton concentration at the opposite side was varied. The simulation was carried out using method B (total number of events: $5\cdot10^5$) with $N_s=10$ and $f=10^{-21}$ J s; the other parameter values are given in Table 1

Results

Examples of simulations using the parameter values of Table 1 are represented in Fig. 5 in which the rotation angle ϱ (in units of 2π) is plotted as a function of time t. A fixed driving force $\Delta\psi=\psi'-\psi''=-200$ mV was assumed ($c'=c''=10^{-7}$ M). ϱ was sampled at time intervals of length 500 μs. The rotation angle ϱ increases with time in an irregular fashion, corresponding to a superposition of quasi-continuous rotation and Brownian motion. This behaviour has to be expected, since entry and exit of protons and jumps of stator elements are random processes. The stochastic nature of the motion is a characteristic property of the motor which will be discussed in more detail later.

Dependence of rotation frequency ν and torque M on driving force and viscous load

The mean rotation frequency ν is obtained from the ratio $\varrho(t^*)/2\pi t^*$ taken at a sufficiently long time t^*. In Fig. 6, ν is plotted as a function of protonmotive force Δp defined by

$$\Delta p\equiv\Delta\psi+\frac{kT}{e_0}\ln\frac{c'}{c''}=\Delta\psi-(59\text{ mV})\,\Delta\text{pH}. \tag{34}$$

$\Delta\text{pH}\equiv\text{pH}'-\text{pH}''$ is the pH difference between intra- and extracellular medium. In the upper curve of Fig. 6, the driving force Δp was assumed to be purely electric ($\Delta p=\Delta\psi$; $c'=c''$). In this case the rotation frequency increases nearly linearly with Δp, up to at least -200 mV. A totally different dependence of ν on Δp is observed when the driving force is purely osmotic ($\Delta\psi=0$), as seen from the middle and lower curve of Fig. 6. The middle curve has been calculated with fixed cytoplasmic proton concentration $c'=10^{-6}$ M and variable extracellular concentration $c''\geq c'$. In the simulation represented by the lower curve, the extracellular concentration $c''=10^{-6}$ was held constant and the cytoplasmic concentration $c'\leq c''$ was varied. In both cases the rotation frequency approaches limiting values at large protonmotive force. According to (21)–(23), the saturation behaviour for $c'=$const. results from the fact that in the limit of large c'' the probabilities of states A_0, B_0, A_{n+1} and B_{n+1} approach constant values $p(A_0)\approx p(B_0)\approx p(A_{n+1})\approx 0$, $p(B_{n+1})\approx 1$. Similarly, for $c''=$const. and $c'\to 0$, the relations $p(A_0)\approx p(A_{n+1})\approx 1/12$, $p(B_0)\approx 0$, $p(B_{n+1})\approx 10/12$ hold for $c''/K''=10$ and $H=1$. In the limit of small $\Delta p(|\Delta p|\ll kT/e_0\approx 26$ mV) electric and osmotic driving forces become kinetically equivalent, as may be expected.

It is important to note that the range in which ν is a linear function of Δp depends on the viscous load. If the simulations are carried out under the same conditions as in Fig. 6, but with a much higher friction coefficient ($f=10^{-19}$ J s), the rotation frequency is found to be proportional to Δp up to about -120 mV, irrespective of whether the driving force is electric or osmotic (not shown).

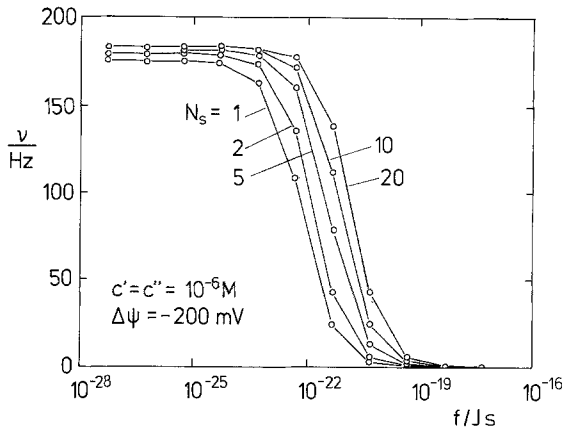

Fig. 7. Rotation frequency ν as a function of friction coefficient f for different numbers N_s of stator elements. The simulations were carried out for symmetrical proton concentrations ($c'=c''=10^{-6}$ M) and a driving force $\Delta p=\Delta\psi=-200$ mV. The other parameters are given in Table 1

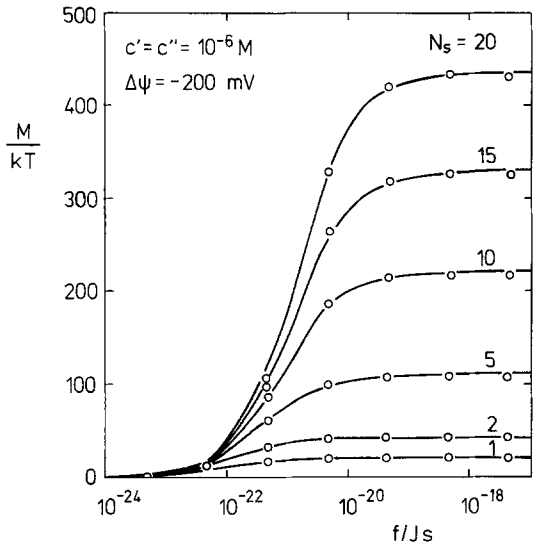

Fig. 8. Torque M generated by the motor (in units of $kT\approx 4.1\cdot 10^{-21}$ J) as a function of friction coefficient f, with the number N_s of stator elements as variable parameter. $\Delta\psi=-200$ mV, $c'=c''=10^{-6}$ M; the other parameters are given in Table 1

As discussed previously, the friction coefficient f may be varied experimentally over a wide range, from $f\leq 5\cdot 10^{-22}$ J s for flagella rotating freely in a low-viscosity medium, up to $f\approx 5\cdot 10^{-20}$ J s for tethered cells. In Fig. 7 the dependence of rotation frequency ν on f is represented with the number N_s of stator elements as a variable parameter. With decreasing friction coefficient f, the rotation frequency increases towards an asymptotic value ν_0. This limiting frequency ν_0 is a function of the jumping rate constants $\tilde{k}$ and $\tilde{l}$ of the stator elements (not shown). Thus, ν_0 reflects the internal friction of the motor resulting from the resistance which has to be overcome in the relative motion of stator elements with respect to the rotor.

Interestingly, the limiting frequency ν_0 depends on the number N_s of stator elements (Fig. 7). This behaviour is likely to result from the fact that the individual stator

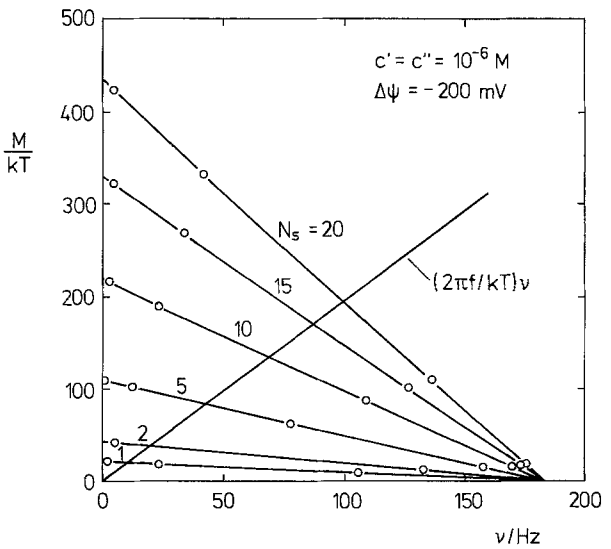

Fig. 9. Torque M (in units of kT) as a function of rotation frequency ν. The values of the parameters were the same as in Fig. 7. $M(\nu)$ has been obtained from the data of Fig. 7 using the relation $M=2\pi\nu f$

elements are not strictly independent of each other, but coupled through the motion of the rotor.

At vanishing external torque M_e, the torque M generated by the motor may be obtained from the rotation frequency ν at a given friction coefficient f (Fig. 7), according to the relation $M=2\pi\nu f$ (compare (25)). Alternatively, M may be evaluated from the mean displacement angle $\langle\gamma\rangle$ of the stator elements, using the relation $M=-q N_s\langle\gamma\rangle$ (3). Within the limits of statistical error, both methods gave identical results. In Fig. 8 the torque M is represented as a function of friction coefficient f for different values of N_s. At low friction, the torque vanishes (as it must), whereas in the limit of high friction, the torque becomes constant. This limiting value $M(f\to\infty)\equiv M_0$, sometimes referred to as the stall torque, is equal to the torque which has to be applied externally to stop the motor.

For comparison with experimental results (see below) it is convenient to plot the torque M as a function of rotation frequency ν (Fig. 9). M is found to be a nearly linear function of ν and thus can be represented by

$$M(\nu)\approx M_0(1-\nu/\nu_0) \tag{35}$$

where M_0 is the stall torque and ν_0 the limiting frequency at vanishing viscous load. For a given fixed friction coefficient f, the rotation frequency can be obtained from the intersection point of the straight line $M=2\pi\nu f$ with $M(\nu)$ in Fig. 9.

Values of ν evaluated in this way from Fig. 9 for fixed friction coefficient are found to be proportional to the number N_s of stator elements at high friction ($\nu\to 0$). This agrees with the experimental observation (Blair and Berg 1988) that ν increases in regular steps when N_s is increased biosynthetically.

It is instructive to evaluate, on the basis of (3), the average deflection angle $\langle\gamma\rangle$ of the stator elements. In the limit of low external friction ($M=0$), $\langle\gamma\rangle$ vanishes, whereas under stall conditions, $\langle\gamma\rangle$ becomes maximal and

equal to $M_0/q\,N_s$. From the results of Fig. 9, the maximum value of $\langle\gamma\rangle$ is estimated to be 0.22, or 13°, at a driving force of −200 mV.

Dependence of M and v on proton concentration

The torque generated by the motor depends on the aqueous proton concentration. This is illustrated by Fig. 10 in which M is plotted as a function of v for different values of c/K under the condition $c'=c''\equiv c$. Both the stall torque $M_0\equiv M(v=0)$ as well as the limiting rotation frequency $v_0\equiv v(M=0)$ are found to decrease with decreasing values of c/K, i.e., with decreasing occupancy of the proton-binding sites. As seen from Fig. 11, the dependence of v_0 on proton concentration c can be approximately fitted with a Michaelis-Menten equation of the form

$$v_0=v_0^{\max}\frac{c}{c+K_M} \tag{36}$$

where K_M is the ion concentration at which v_0 becomes equal to $v_0^{\max}/2$.

The maximum value of the stall torque, $M_0^{\max}$, obtained by numerical simulation in the limit $c\gg K$, may be compared with theoretical predicitons. If the proton-binding sites are always occupied, the number of protons translocated in a single revolution is equal to $N_r N_s$, corresponding to a change of free energy of magnitude $N_r N_s e_0 \Delta p$. This energy must be equal to the mechanical energy per revolution, $-2\pi M_0^{\max}$. Thus:

$$M_0^{\max}=-N_r N_s e_0 \Delta p/2\pi. \tag{37}$$

With the parameters used for the simulations of Fig. 11 ($N_r=20$, $N_s=10$, $\Delta p=-200$ mV), the predicted value of $M_0^{\max}/\mathrm{kT}$ becomes equal to 248, which agrees with the result of Fig. 11.

Furthermore, according to (37), the maximum torque should be proportional to the number N_s of stator elements. This prediction is borne out by the simulations represented in Fig. 9.

Effects of elastic restoring force

According to (2), the elastic restoring force acting on a stator element is decribed by the force constant q. The dependence of rotation frequency v on q is represented in Fig. 12. It is seen that v is independent of q at low values of the force constant, but strongly decreases at large q. This behaviour can be understood in the following way. When a stator element moves from its equilibrium position (deflection angle $\gamma=0$) to an adjacent potential well, an activation energy of magnitude $q(\Delta\gamma)^2/2$ is required to overcome the elastic restoring force; $\Delta\gamma$ is the deflection angle corresponding to the position at the top of the energy barrier. If the energy wells are regularly spaced and if the barriers are symmetrical, $\Delta\gamma$ becomes equal to $\pi/N_r(n+1)$ where n is the number of internal energy wells (Fig. 3). Accordingly, in the presence of an elastic restoring force, the frequency of jumps over the energy barriers

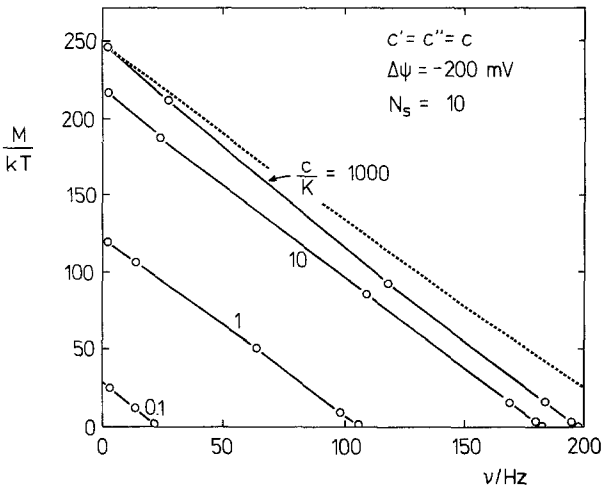

Fig. 10. Torque M (in units of kT) as a function of rotation frequency v for different values of the ratio c/K. $c'=c''=c$, $\Delta\psi=-200$ mV, $N_s=10$; the other parameters are given in Table 1. Dashed line: values predicted from the previous analytical treatment (Läuger 1988) for $c/K=1000$

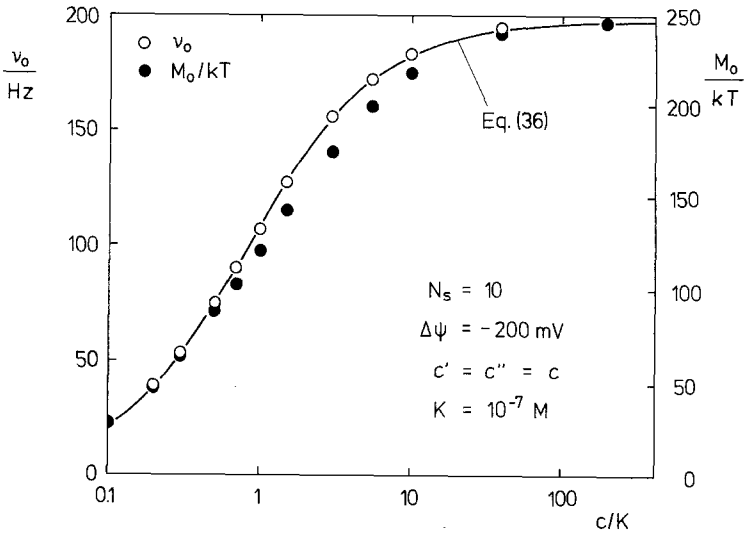

Fig. 11. Zero-load rotation frequency $v_0\equiv v\,(M=0)$ and stall torque $M_0\equiv M(v=0)$ as a function of c/K. $c'=c''=c$, $\Delta\psi=-200$ mV, $N_s=10$; the other parameter values are given in Table 1. The line has been drawn according to (36) with $v_0^{\max}=198$ Hz and $K_M/K=0.835$

is reduced by a factor λ:

$$\lambda\equiv\exp\left[-\frac{q}{2\,\mathrm{kT}}(\Delta\gamma)^2\right]=\exp\left[-\frac{\pi^2 q}{2\,\mathrm{kT}\,N_r^2(n+1)^2}\right]. \tag{38}$$

Thus, at large values of q, the rotation frequency should exponentially decrease with increasing q. On the other hand, when the exponent in (38) is small compared to unity, v is predicted to become independent of q. With $N_r=20$ and $n=5$, this should be the case for $q\ll 10^{-17}$ J, in agreement with the results of Fig. 12.

The experimental value of the force constant, which has been used in most simulations, $q=4\cdot 10^{-19}$ J s (Table 1), lies in the range where M is only weakly dependent on q (Fig. 12).

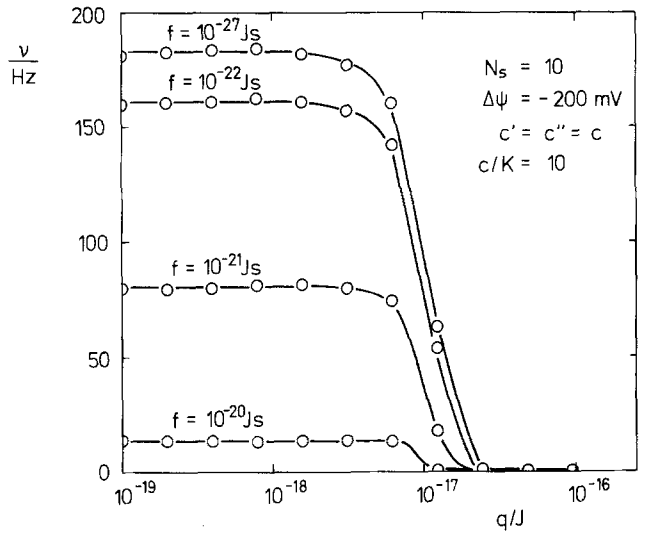

Fig. 12. Rotation frequency ν as a function of force constant q for different values of the friction coefficient f. $N_s=10$, $c'=c''\equiv c$, $c/K=10$, $\Delta\psi=-200$ mV. The other parameter values are given in Table 1

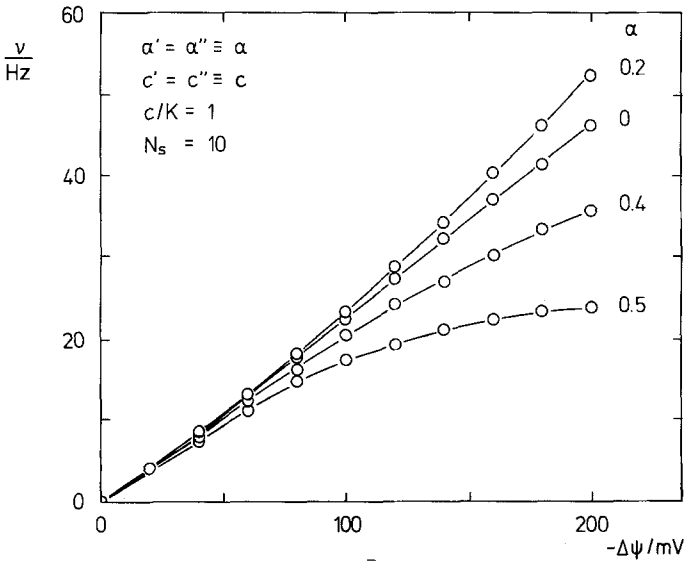

Fig. 13. Rotation frequency ν as a function of voltage $\Delta\psi$. $\alpha'=a'/h$ and $\alpha''=a''/h$ are the relative lengths of the access channels ("ion wells") connecting the entrance sites for H^+ with the adjacent aqueous solutions (Fig. 1). $N_s=10$, $c'=c''\equiv c$, $c/K=1$. The other parameter values are given in Table 1. The voltage dependence of the equilibrium dissociation constants K' and K'' was evaluated according to (7) and (8) with $\tilde{K}'=\tilde{K}''\equiv K$ and $\alpha'=\alpha''\equiv\alpha$

Ion-well effects

When part of the transmembrane voltage drops across an access channel connecting the binding site with the adjacent aqueous solution, the binding affinity for H^+ becomes a function of voltage, i.e., the access channel acts as an "ion well". Simulations allowing for the presence of ion wells are represented in Fig. 13. The relative depths of the wells at the cytoplasmic and extracellular side are denoted by α' and α'', respectively (7) and (8). The simulations were carried out under the condition $\alpha'=\alpha''\equiv\alpha$, $\tilde{K}'=\tilde{K}''\equiv K$ and $c'=c''\equiv c$. For $\alpha=0$ (access channels absent), the rotation frequency ν is a nearly linear function of voltage $\Delta\psi$. For $\alpha=0.2$, ν is increased and becomes slightly superlinear. For $\alpha=0.4$ and 0.5, the rotation frequency is again smaller and tends to saturate at large voltages. This saturation behaviour results from the fact that for $\alpha'=\alpha''\approx 0.5$ nearly all the total voltage drops across the access channels, so that the rate constants for jumps of the stator elements become virtually voltage-independent. The saturation behaviour of ν is even more pronounced for larger values of c/K (not shown). The limiting case $\alpha'=\alpha''=0.5$ corresponds to the model of Meister et al. (1989) in which the transmembrane voltage has been assumed to act exclusively via an ion-well effect.

Proton flux and coupling ratio

In the model discussed here, the individual stator elements are allowed to move independently of the movement of the rotor. This has the consequence that coupling between proton flow and rotation is, in general, not perfect. If the rotor is held fixed, a given stator element may still carry out transitions between the states of the reaction cycle (Fig. 4), and occasionally may complete the whole cycle, taking up a proton on one side ($A_0\rightarrow B_0$), releasing it to the other side ($B_{n+1}\rightarrow A_{n+1}$) and returning back in unloaded form ($A_{n+1}\rightarrow A_n\rightarrow A_0$). Such a carrier-like behaviour of stator elements may be expected to be most pronounced at high friction and at nonsaturating proton concentrations ($c'\lesssim K'$, $c''\lesssim K''$), when states with empty binding site have a non-zero probability.

Since $N_r N_s$ is the number of elementary translocation events associated with a single revolution, the rate by which rotation-linked translocation events occur is equal to $N_r N_s \nu$. Accordingly, coupling beween rotation and proton flow may be described by the coupling ratio Q which is defined by the ratio of $\nu N_r N_s$, divided by the net proton flux J_H:

$$Q\equiv\frac{N_r N_s \nu}{J_H}. \tag{39}$$

For Q to be positive, ν and J_H have to be taken as absolute values. In the simulation, J_H is obtained as the difference in the number of protons entering and leaving the motor per unit time at the cytoplasmic side.

The coupling ratio Q is represented in Fig. 14 as a function of friction coefficient f for different values of proton concentration $c'=c''\equiv c$ and of the ratio $\tilde{k}/\tilde{l}$ of jumping frequencies in the empty ($\tilde{k}$) and the occupied state ($\tilde{l}$). For all combinations of $\tilde{k}/\tilde{l}$ and c/K, the coupling ratio Q approaches zero in the limit of high friction coefficient f. This results from the above-mentioned carrier-like behaviour of the stator elements which causes the proton flux I_H to remain finite for vanishing rotation frequency ν. Under conditions of low friction and saturating ion concentration, the proton flux J_H must become equal to $N_r N_s \nu$, so that Q approaches unity. This is borne out by the simulation, as seen from the curve for $c/K=1000$ in Fig. 14A.

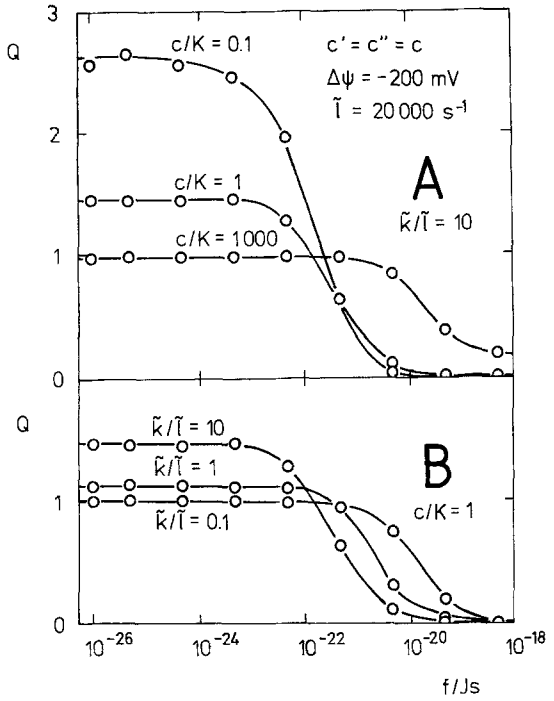

Fig. 14 A, B. Coupling ratio $Q = v\, N_r\, N_s/J_H$ as a function of friction coefficient f for different values of the ratio $\tilde{k}/\tilde{\Gamma}$ of the jumping frequencies in the empty ($\tilde{k}$) and in the occupied state ($\tilde{\Gamma}$). $\tilde{\Gamma}$ was held fixed at $2 \cdot 10^4\ s^{-1}$. $N_s = 10$, $c' = c'' = 10^{-7}$ M, $\Delta\psi = -200$ mV. The other parameter values are given in Table 1. **A** variation of c/K at $\tilde{k}/\tilde{\Gamma} = 10$; **B** variation of $\tilde{k}/\tilde{\Gamma}$ at $c/K = 1$

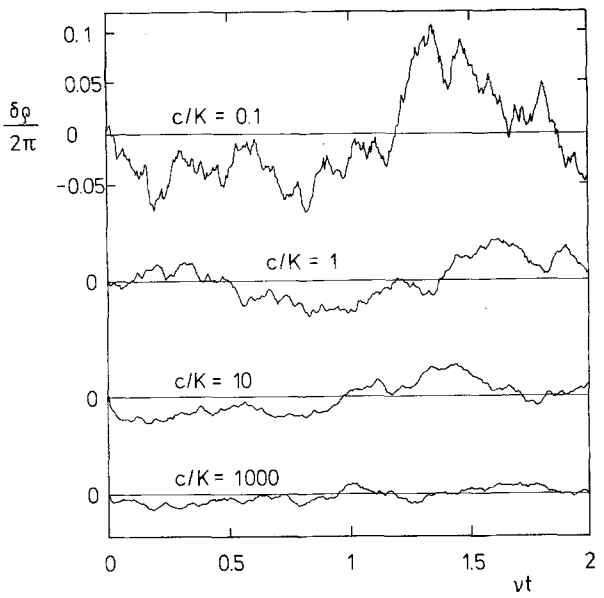

Fig. 15. Stochastic behaviour of the motor. The difference $\delta\varrho(t) \equiv \varrho(t) - 2\pi\nu t$ between the rotation angle ϱ and its expectation value $2\pi\nu t$ is plotted on the ordinate in units of 2π. The simulations were carried out using method A with time steps $\Delta t = 2.5$ μs. $c' = c'' \equiv c$, $\Delta p = \Delta\psi = -200$ mV, $N_s = 10$, $f = 10^{-21}$ J s. The other parameters are given in Table 1. The mean rotation frequency ν was determined in a separate simulation over an extended time period under otherwise identical conditions; ν varied between 10.2 Hz ($c/K = 0.1$) and 86 Hz ($c/K = 1000$). The ordinate scale is the same in all cases

At non-saturating ion concentrations, Q may assume values larger than unity. This may be understood by considering the following limiting case. Assume that external friction is negligible ($f \approx 0$) and that the ion concentration c is so small that no more than one out of N_s stator elements is occupied by an ion at any time. In this case, every proton passing through the motor leads to rotation of the rotor by an angle $\Delta\varrho = 2\pi/N_r$, so that the rotation frequency ν becomes equal to J_H/N_r, yielding $Q = N_s$. Thus, under the conditions of Fig. 14 A, the coupling ratio may be expected to approach the value $Q = N_s = 10$ in the limit $f \to 0$ and $c/K \to 0$. By the same token, $Q = N_s$ represents an upper limit for the coupling ratio, since the minimum number of protons required to drive the rotor through one revolution is equal to N_r.

If transitions with empty binding site are kinetically inhibited ($\tilde{k} \ll \tilde{\Gamma}$), proton flux and rotation become completely coupled. This explains the finding (Fig. 14 B) that in the limit of low friction, Q approaches unity for $\tilde{k}/\tilde{\Gamma} = 0.1$.

Stochastic properties

Since force is generated in a small number of units (the stator elements), the operation of the motor is necessarily subjected to random fluctuations. Stochastic fluctuations of rotation rate may originate from at least two different sources. In the absence of an external driving force, the rotor carries out Brownian rotational diffusion resulting from random jumps of stator elements. Brownian rotation of the motor may be described by a rotational diffusion coefficient D_{rot} (Berg 1983):

$$D_{\text{rot}} = \frac{\langle(\Delta\varrho)^2\rangle}{2\,\Delta t}. \tag{40}$$

$\langle(\Delta\varrho)^2\rangle$ is the mean square deviation of the rotation angle ϱ within time interval Δt.

At finite driving force Δp, an additional component appears in the random behaviour of $\varrho(t)$, resulting from fluctuations in the occupancy of ion-binding sites. This is obvious in the case where the driving force is purely electric ($c' = c'' \equiv c$, $\Delta p = \Delta\psi$). Under this condition fluctuations in the number of bound ions lead to random variations of the force acting on the motor. Large fluctuations of binding-site occupancy may be expected at non-saturating proton concentrations ($c \lesssim K$).

For representing the stochastic time-behaviour of rotation angle ϱ, it is convenient to plot the quantity $\delta\varrho$ as a function of νt:

$$\delta\varrho(t) \equiv \varrho(t) - 2\pi\nu t \tag{41}$$

where $2\pi\nu t$ is the expectation value of rotation angle ϱ at time t; the mean rotation frequency ν is obtained (as before) as the limiting value of the ratio $\varrho(t^*)/2\pi t^*$ for $t^* \to \infty$. $\delta\varrho(t)$ is plotted in Fig. 15 over a time interval of two rotation periods ($0 \le \nu t \le 2$) for different values of c/K. It is seen that the rotation is comparatively smooth at large c/K, but becomes increasingly irregular with de-

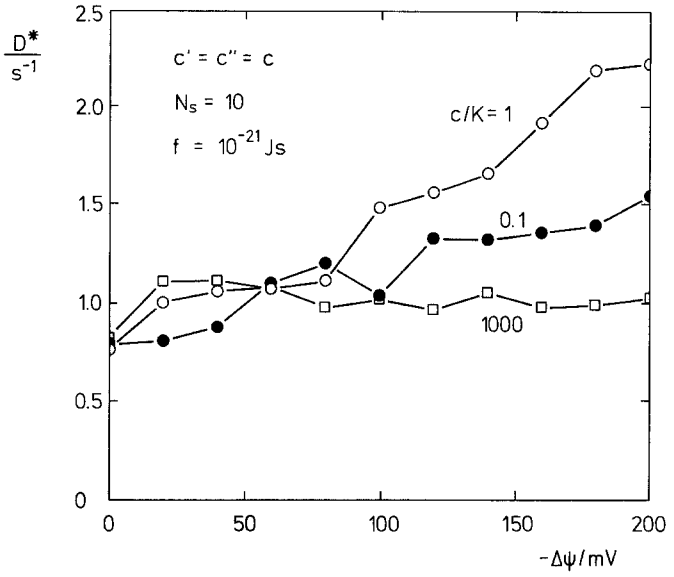

Fig. 16. Generalized rotational diffusion coefficient D^* (42) as a function of driving force $\Delta p = \Delta\psi$ for three different values of c/K under the condition $c' = c'' \equiv c$, $N_s = 10$, $f = 10^{-21}$ J s. The other parameters are given in Table 1. The rotation angle $\varrho(t)$ was obtained by simulation using method A with time increments of 2.5 μs. Angle increments $\Delta\varrho$ (42) were taken at time intervals $\Delta t = 5$ ms. The mean rotation frequency v was determined from the total angle ϱ^* at the end of the simulation period of length $t^* = 2.5$ s according to $v = \varrho^*/2\pi t^*$. The value of D^* was independent of Δt for $\Delta t > 2.5$ ms, but decreased to zero for $\Delta t \to 0$

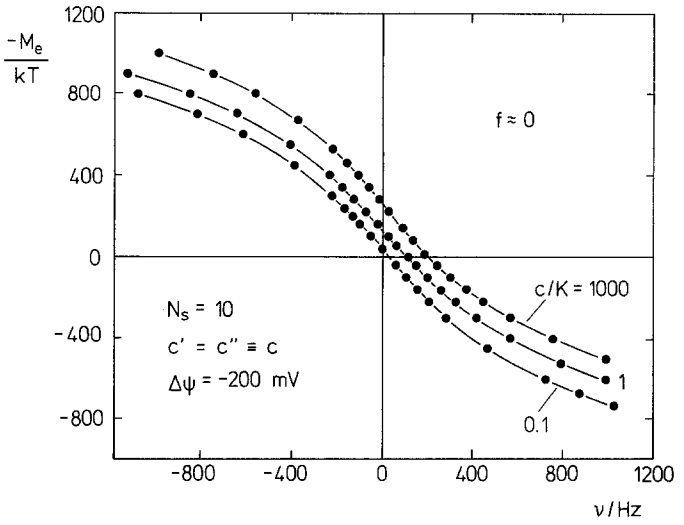

Fig. 17. Dependence of rotation frequency v on externally-applied torque M_e for different values of c/K. For easy comparison with Fig. 10, $-M_e/\mathrm{kT}$ is plotted as a function of v. The simulations were carried out for vanishing friction coefficient (using a value of $f = 10^{-25}$ J s), $N_s = 10$, $c' = c'' \equiv c$ and $\Delta\psi = -200$ mV; the other parameters were taken from Table 1

creasing ion concentration c. In the limit $c/K \to 0$ in which the average driving force vanishes, the motor exhibits pure rotational diffusion.

For further analysis of the stochastic behaviour of the motor we introduce the quantity

$$D^* \equiv \frac{1}{2\Delta t}\langle(\Delta\varrho - 2\pi v \Delta t)^2\rangle \tag{42}$$

where $\Delta\varrho$ is the increment of ϱ during time Δt; the averaging is to be carried out over many time intervals of length Δt in the course of the simulation. Comparison with (40) shows that D^* should become equal to D_{rot} at vanishing driving force ($v = 0$). Thus, D^* may be considered as a generalized rotational diffusion coefficient accounting for fluctuations of force under non-equilibrium conditions.

The quantity D^* is represented in Fig. 16 as a function of protonmotive force $\Delta p = \Delta\psi$ for different values of c/K. D^* increases with $-\Delta\psi$ for $c/K = 1$, but remains virtually constant both at low (0.1) and high values (1000) of c/K. This behaviour may be explained in the following way. At low proton concentration ($c \to 0$), the binding sites are mostly empty so that the stochastic motions of the rotor become independent of $\Delta\psi$, corresponding to pure rotational diffusion. At high values of c/K, the binding sites are always occupied and fluctuations in occupancy are negligible. Thus, at large c/K, D^* should again approach the rotational-diffusion limit. At intermediate values of c/K, the stochastic behaviour of the motor is influenced by fluctuations in binding-site occupancy which lead to fluctuations of driving force at $\Delta\psi \neq 0$. Since in the simulations represented in Fig. 16, the rate constants for jumps of stator elements with empty and occupied binding site have been assumed to be the same ($\tilde{k} = \tilde{l}$), the values of D^* for $c/K \ll 1$ and $c/K \gg 1$ should approximately agree, which is indeed observed.

The limit of D^* at low protonmotive force may be compared with predicted values of the rotational diffusion coefficient D_{rot}. At vanishing external friction ($f = 0$) and for $N_s = 1$, D_{rot} should be determined by the jumping frequency $\tilde{k} = \tilde{l}$ of the stator element and by the angle increment $\varrho_0 = 2\pi/(n+1)N_r$ in a single jump. In analogy to linear diffusion (Berg 1983), D_{rot} is given by

$$D_{\mathrm{rot}} = \frac{1}{2}\tilde{k}\,\varrho_0^2 = \frac{2\pi^2\,\tilde{k}}{(n+1)^2\,N_r^2}. \tag{43}$$

For $\tilde{k} = 2 \cdot 10^4\ \mathrm{s}^{-1}$, $n = 5$ and $N_r = 20$, D_{rot} is predicted to be $27\ \mathrm{s}^{-1}$. This value may be compared with the result of simulations carried out with the same parameter values, yielding $D^* \approx 50\ \mathrm{s}^{-1}$ for $N_s = 1$, $f \approx 0$ and $\Delta p = 0$. Thus, the rotational diffusion coefficient determined by simulation agrees within an order of magnitude with the value predicted from (43). (The difference between D_{rot} and D^* may result from the elastic restoring forces acting on the stator element, which are not taken into account in (43)).

Externally-applied torque M_e

Valuable information on the properties of the motor may be expected from experiments in which an external torque M_e is applied in addition to the torque generated by the protonmotive force Δp. Such experiments may become possible in the future (Meister et al. 1989). In Fig. 17 the relationship between rotation frequency v and external torque M_e is represented under the condition of vanishing

viscous load ($f \approx 0$) for fixed protonmotive force $\Delta p = \Delta\psi$. For easy comparison with the results shown in Fig. 10, $-M_e/\mathrm{kT}$ is plotted as a function of v. At vanishing external torque M_e, the flagellum rotates counterclockwise ($v = v_0 > 0$) under the influence of the protonmotive force. For $-M_e < 0$, the external torque has the same direction as the motor-generated torque, and the rotation frequency increases beyond v_0. If $-M_e$ is equal to the stall torque M_0, rotation ceases ($v = 0$). For more positive values of $-M_e$, the flagellum rotates in reverse direction ($v < 0$). As seen from Fig. 17, the rotation frequency v increases with M_e in a superlinear fashion at large positive or negative values of M_e. This non-linear behaviour of $v(M_e)$ can be explained in the following way. At large torque, the stator elements are strongly deflected from their equilibrium position, so that the restoring force $-q\gamma_i$ (2) becomes large. Since the rate constants k_j', k_j'', l_j' and l_j'' depend exponentially on $q\gamma_i$ (11–15), the rotation frequency varies non-linearly with M_e.

In experiments with free-swimming or tethered cells in the absence of an externally-applied torque, the equivalent of M_e is the frictional torque $-f\omega$ which counteracts the torque M generated by the motor. It is thus interesting to compare the numerical values of $M(v)$ obtained under the condition $M_e = 0$ with the values of $-M_e(v)$ obtained under the condition $f = 0$. It is found that $M(v)$ from Fig. 10 and $-M_e(v)$ from Fig. 17 agree, within the limits of statistical error, in the whole range of M and v ($0 \le M \le M_0$; $0 \le v \le v_0$) (not shown).

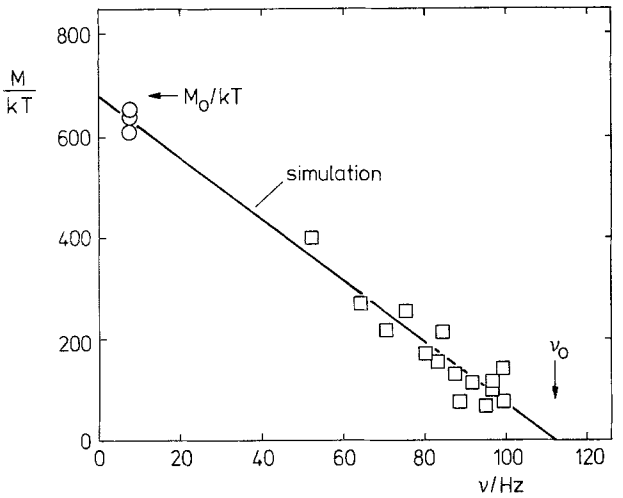

Fig. 18. Comparison with experimental results: Torque M generated by the flagellar motor as function of rotation rate v. M is referred to a single flagellum and is given in units of $\mathrm{kT} \approx 4.1 \cdot 10^{-21}$ J (at 22 °C). *Squares*: experiments with free-swimming cells of Streptococcus in media of different viscosity at constant protonmotive force (Lowe et al. 1987; Meister et al. 1989). *Circles*: experiments with tethered cells (Manson et al. 1980). M_0 and v_0 are the limiting values of M and v at high and low viscous load, respctively. The straight line was obtained by numerical simulation of the model, using the following parameter values: $N_r = 47$, $N_s = 16$, $n = 5$, $c' = c'' = 10^{-7}$ M, $K' = K'' = 10^{-8}$ M, $H = 1$, $\tilde{k} = \tilde{l} = 4 \cdot 10^4\ \mathrm{s}^{-1}$, $q = 4 \cdot 10^{-19}$ J, $\Delta\psi = -150$ mV, $T = 295$ K

Comparison with experimental results

The dynamic properties of a rotary motor may be characterized by the relationship between rotation frequency v and torque M. The best information on $M(v)$ available so far is provided by the experiments of Lowe et al. (1987) with Streptococcus cells (Fig. 18). An approximately linear dependence of M on v was observed which can be represented by the relation $M = M_0(1 - v/v_0)$. Thus, at high friction, the motor runs at constant torque, and at low friction, at constant speed (Berg and Khan 1983). As shown above (Figs. 9 and 10), the linear dependence of M on v is reproduced by the numerical simulation. A fit of the model to the experimental results (Fig. 18) is obtained with the following parameter values: $N_r = 47$, $N_s = 16$, $n = 5$, $c' = c'' \equiv c = 10^{-7}$ M, $K' = K'' \equiv K = 10^{-8}$ M, $H = 1$, $\tilde{k} = \tilde{l} = 4 \cdot 10^4\ \mathrm{s}^{-1}$, $q = 4 \cdot 10^{-19}$ J, $\Delta\psi = -150$ mV, $T = 295$ K. This set of parameter values is, of course, not unique. Within the framework of the model considered here, a linear relation between M and v may be generally expected, provided that the number n of ion binding sites is chosen to be larger than 2–3 (Läuger 1988). Since saturation of the proton-binding sites has been assumed ($c/K = 10$), the stall torque M_0 is given by the relation $M_0 \approx M_0^{\max} = -N_r N_s e_0 \Delta p / 2\pi$ (37); therefore, M_0 directly yields the product $N_r N_s$. From the experimental values $M_0 \approx 690 \cdot \mathrm{kT}$ and $\Delta p = -150$ mV, $N_r N_s$ is estimated to be ≈ 750. Thus, with $N_s = 16$ (Block and Berg 1984), N_r has to be chosen to be ≈ 47; if the lower value, $N_s = 8$ (Blair and Berg 1988), is used, N_r becomes equal to 94. With a ring diameter of 30 nm, $N_r = 94$ would mean that the distance between adjacent half-channels on the periphery of the rotor is about 1 nm.

Since $N_r N_s$ is equal to the number of protons translocated in a single revolution, an independent estimate of $N_r N_s$ is obtained from experiments in which the proton flux through the motor has been determined (Meister et al. 1987). This yields a value of about 1240 for $N_r N_s$.

The dependence of rotation frequency v on protonmotive force Δp has been studied with two different cell types. v was found to increase linearly with membrane voltage $\Delta\psi$ up to 80 mV in *Streptococcus* (Khan et al. 1985). In *Streptococcus* (Manson et al. 1980) and in *Bacillus subtilis* (Khan and Macnab 1980; Shioi et al. 1980), the electrical ($\Delta\psi$) and the osmotic (ΔpH) components of Δp are almost equally effective in driving flagellar rotation. This behaviour is predicted by the model at high viscous load (not shown). In *Bacillus subtilis*, the rotation frequency was found to saturate above 60 to 100 mV (Khan and Macnab 1980; Manson et al. 1980; Shioi et al. 1980; Khan and Berg 1983); saturation was observed both for $\Delta p = \Delta\psi$ and for $\Delta p = -(\mathrm{kT}/e_0)\,\Delta$pH (Khan and Macnab 1980). A possibility for explaining the equivalence of $\Delta\psi$ and ΔpH, as well as the saturation at large Δp, derives from the assumption that the access channels connecting the binding sites to the aqueous phase act as ion wells. Saturation of rotation frequency v at large driving force Δp is clearly seen in the simulations represented in Fig. 13 in which ion-well effects (α', $\alpha'' > 0$) have been accounted for.

Information on stochastic fluctuations of rotation rate is scanty so far. For the representation of experimental results it is convenient to introduce the standard deviation σ_τ of the duration τ of a rotation period:

$$\sigma_\tau^2 = \langle(\tau - \bar{\tau})^2\rangle \tag{44}$$

where $\bar{\tau} = 1/\nu$ is the average duration of a rotation period. σ_τ is related to the standard deviation σ_ϱ of rotation angle ϱ after time $t = \bar{\tau}$ according to $\sigma_\tau/\bar{\tau} \approx \sigma_\varrho/2\pi$. Together with (42) this gives

$$\frac{\sigma_\tau}{\bar{\tau}} \approx \frac{1}{2\pi}\sqrt{2D^*\bar{\tau}}\,. \tag{45}$$

In the experiments with tethered cells, rotation was found to be remarkably regular, with values of $\sigma_\tau/\bar{\tau}$ of about 0.09 (Khan et al. 1985). This corresponds, with the experimentally observed rotation frequency of $\nu = 1/\bar{\tau} \approx 2$ Hz, to $D^* \approx 0.3\ \mathrm{s}^{-1}$, a value which is close to the estimated rotational diffusion coefficient of Streptococcus cells in water. This means that under the given experimental conditions, contributions to σ_τ from fluctuations of binding-site occupancy are negligible. According to Fig. 16, larger fluctuations of rotation rate may be expected at sub-saturating proton concentrations.

Discussion

The microscopic model of the bacterial flagellar motor analysed above is based on the notion that ions passing through the motor use a channel-like pathway formed by ligand groups located partly on the rotor, partly on the stator elements. In a previous paper (Läuger 1988), an analytical treatment of this model was described which required a number of simplifying assumptions. In particular, the analysis had to be restricted to saturating proton concentrations in order to derive an analytical expression for the dependence of rotation rate on experimental variables (f, $\Delta\psi$, c', c''). Furthermore, effects of elastic restoring forces acting the stator elements could only indirectly be accounted for. The present treatment is free from these restrictions, since a computer simulation can provide, at least in principle, a complete description of a molecular system.

Mechanisms of flagellar rotation involving loose coupling between proton flow and rotation have been analysed by Oosawa and coworkers (1982, 1983) and by Kobayashi (1988). Recently, a model which has some similarity with the model discussed here has been treated by Meister et al. (1989). In the mechanism considered by Meister et al., the membrane voltage acts exclusively on ion movement across the access channels, while ion translocation between binding sites on the rotor and the concomitant lateral movement of the stator element are assumed to be voltage-independent processes. This corresponds to the limiting case $\beta = 0$ in our model. Another difference between the two models lies in the fact that Meister et al. have assumed strict coupling between proton flow and rotation, whereas in the mechanism discussed here, the coupling ratio can be larger or smaller than unity.

The numerical simulations carried out in this study yield the rotation frequency ν as a function of driving force Δp at arbitrary (saturating and non-saturating) proton concentrations c' and c''. For large values of c' and c'' and small force constant q (see below), the results approximately agree with the predictions from the previous analytical treatment (Läuger 1988) which was based on the assumption of kinetic independence of the stator elements and which was restricted to the limiting case $c' \gg K'$, $c'' \gg K''$. This is seen in Fig. 10 in which the dashed line indicates the result from the analytical treatment for $c/K = 1000$ and $N_s = 10$.

At sub-saturating proton concentrations ($c \leq K$) and for a given protonmotive force $\Delta p = \Delta\psi$, both the zero-load rotation frequency ν_0 and the stall torque M_0 decrease with decreasing values of c/K (Fig. 11). This finding is consistent with the notion that for $\Delta p = \Delta\psi$ the average force acting on the motor is proportional to the number of ions occupying the binding sites. In models in which rotation and proton flow are assumed to be strictly coupled (Läuger 1988; Meister et al. 1989), the stall torque is always given by a thermodynamic relation of the form $M_0 = -N_r N_s e_0 \Delta p/2\pi$ which, for $\Delta p = \Delta\psi$, does not depend on ion concentration c (compare (37)). The model considered here accounts for the possibility that stator elements move with empty proton binding site, a process which leads to uncoupling (or "slippage"). Thus, measuring the stall torque as a function of ion concentration yields information on the degree of coupling. More direct information on the thermodynamic efficiency of the motor is obtained from the coupling ratio $Q = \nu N_r N_s/J_H$ represented in Fig. 14. Q is found to depend on microscopic parameters of the model, such as the ratio $\tilde{k}/\tilde{l}$ of the jumping frequencies in the empty and occupied state of the channel, as well as on experimental variables such as ion concentration and viscous load.

The thermodynamic efficiency η of the motor is defined as the rate of generation of mechanical energy, $2\pi\nu M$, divided by the rate of energy dissipation by downhill proton flow, $e_0 \Delta p J_H$:

$$\eta = \frac{2\pi\nu M}{e_0 \Delta p J_H} = \frac{2\pi M Q}{N_r N_s e_0 \Delta p} \tag{46}$$

(again, ν, M, Δp and J_H are to be taken as absolute values). In Fig. 19, η is represented as a function of friction coefficient f for different values of c/K. At low viscous load, η vanishes, since for $f \to 0$ the torque M becomes small. At high viscous load, η becomes again small, since for $f \to \infty$ the rotation frequency approaches zero while the proton flux J_H remains finite. At intermediate values of the friction coefficient, η goes through a maximum. As seen from Fig. 19, the highest efficiency is obtained for saturating proton concentrations ($c \gg K$).

A characteristic feature of the model is the elastic coupling of the stator elements to the cell wall which allows quasi-independent motions of the individual elements (Berg and Khan 1983). Without elastic coupling, rotation of the rotor by one step would require simultaneous tran-

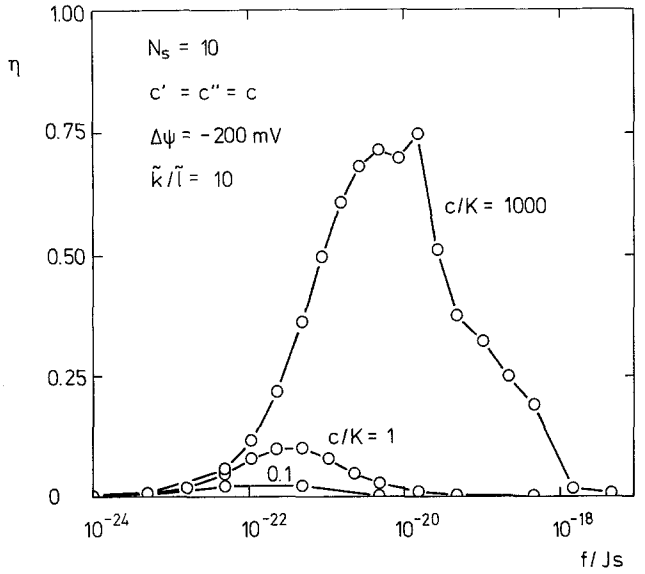

Fig. 19. Thermodynamic efficiency η of the flagellar motor (46) as a function of friction coefficient f. η was calculated for $\tilde{k}/\tilde{l}=10$ under the conditions given in the legend of Fig. 14A

sitions over activation barriers in each of the stator elements, a process which has an intrinsically low probability. In the simulation of the model, the single stator elements were assumed to move independently of each other. The stator elements, however, indirectly interact via motions of the rotor. This interaction leads to the observed dependence of zero-load rotation frequency v_0 on the number N_s of stator elements (Fig. 7). In models in which complete independence of the stator elements is assumed a priori (Läuger 1988; Meister et al. 1989), v_0 is predicted to be independent of N_s, since in this case both the force and the internal friction increase proportional to N_s at vanishing viscous load.

From the foregoing it is clear that the force constant q is an important parameter in the design of a flagellar motor. Strong coupling, corresponding to large values of q, tends to block the motor, as Fig. 12 shows. On the other hand, in the limit of small force constant, the rotation frequency becomes independent of q (Fig. 12). According to (38), the value q_0 below which v becomes constant is given by the condition that the elastic energy $\pi^2 q_0/2N_r^2(n+1)^2$ associated with the transition over a barrier is smaller than kT. For $q<q_0$ the results of the simulation qualitatively agree with the predictions of the analytic treatment (Läuger 1988) in which elastic coupling was not explicitely taken into account.

The simulation method applied in this study is particularly useful for obtaining information on the stochastic properties of the flagellar motor. The random nature of the motion of the rotor is evident from Fig. 15 in which the quantity $\delta\varrho \equiv \varrho - 2\pi v t$ is plotted, representing the deviation of rotation angle ϱ from the expectation value $2\pi v t$. The time course of $\delta\varrho$ which is shown in Fig. 15 for two rotation periods reflects fluctuations of rotation speed resulting from the stochastic nature of the ion binding and release steps and of the motions of the stator elements. Fluctuations of rotation speed are relatively small at high ion concentrations c at which the binding sites are mostly occupied ($c/K \gg 1$), but increase strongly with decreasing values of c/K. (Part of the difference in the behaviour of $\delta\varrho$ at low and at high ion concentration results from the difference in the length of the rotation period $1/v$).

At small driving force, the motion of the rotor may be described as continuous rotation superimposed on rotational diffusion. This is shown in Fig. 16 in which the quantity $D^* \equiv \langle(\Delta p - 2\pi v \Delta t)^2\rangle/2\Delta t$ is plotted as a function of protonmotive force $\Delta p = \Delta\psi$. In the limit of small protonmotive force in which v vanishes, D^* should become equal to the rotational diffusion coefficient $D_{rot} = \langle(\Delta\varrho)^2\rangle/2\Delta t$. D^* is found to be virtually independent of protonmotive force $\Delta\psi$ both at high and at low ion concentration c, but increases with $|\Delta\psi|$ at intermediate concentrations ($c/K=1$). This behaviour may be understood in the following way. At saturating ion concentrations, fluctuations in binding-site occupancy are small so that the stochastic behaviour of the motor is dominated by rotational diffusion. On the other hand, at low ion concentrations at which the binding sites are mostly empty, the average driving force acting on the rotor is small, so that again the protonmotive force has little influence on D^*. At intermediate concentrations ($c \approx K$), fluctuations in binding-site occupancy lead to fluctuations of driving force which increase in amplitude with increasing values of $|\Delta\psi|$.

Acknowledgements. The authors would like to thank Dr. H.-J. Apell and Dr. R. Borlinghaus for helpful discussions. This work has been financially supported by the Deutsche Forschungsgemeinschaft.

Appendix A

Rates of protonation and deprotonation of transport sites at the channel entrance

The rate of protonation of a proton-accepting group R^- at the channel entrance (sites 0 and $n+1$ in Fig. 4) is determined by the following processes:

$$H^+ + R^- \underset{k_{-1}}{\overset{k_1}{\rightleftarrows}} HR \tag{A1}$$

$$H_2O + R^- \underset{k_{-2}}{\overset{k_2}{\rightleftarrows}} OH^- + HR \tag{A2}$$

$$HP + R^- \underset{k_{-3}}{\overset{k_3}{\rightleftarrows}} P^- + HR \tag{A3}$$

(A1) represents protonation by free protons (in the form of H_3O^+), (A2) proton transfer from water molecules, and (A3) proton transfer from the protonated buffer species HP. The buffer P^-/HP is introduced to account for the buffering action by components of the aqueous medium, such as HCO_3^-. The overall rate k_{on} of protonation of R^- is then given by

$$k_{on} = k_1 c_H + k_2 c_w + k_3 c_{HP} \tag{A4}$$

where c_H, c_w and c_{HP} are the concentrations of H_3O^+, H_2O and HP, respectively.

The rate constant k_1 of protonation by free protons may be set equal to the limiting rate constant k_{diff} of a diffusion-controlled reaction (Eigen 1963):

$$k_1 \approx k_{diff} \tag{A 5}$$

For the purpose of an estimate of the order of magnitude, we use in the following the same limiting value k_{diff} for all three reactions (A 1)–(A 3). k_2 and k_3 may be estimated in the following way. The rate constant k_{AB} of the proton-exchange reaction

$$HA + B \xrightarrow{k_{AB}} A + HB \tag{A 6}$$

is given by (Eigen 1963; Schuster 1987):

$$k_{AB} = k_{diff} \frac{K_A}{K_A + K_B} \tag{A 7}$$

$K_A \equiv c_H c_A / c_{HA}$ and $K_B \equiv c_H c_B / c_{HB}$ are the equilibrium dissociation constants of HA and HB. Equation (A 7) states that for downhill protonation ($K_A > K_B$) the reaction is nearly diffusion-limited ($K_{AB} \approx k_{diff}$); if A and B are identical ($K_A = K_B$), the rate constant k_{AB} is reduced by a factor of 2 compared to k_{diff}, since the encounter complex $A-H \cdots B \leftrightarrow A \cdots H-B$ can dissociate with equal probability in either direction. The equilibrium dissociation constant K_R of the transport site may be assumed to be much larger than the dissociation constant of water, $K_w = c_H c_{OH}/c_w \approx 2 \cdot 10^{-16}$ M, so that from (A 7) the relation

$$k_2 c_w \approx k_{diff} c_H c_{OH} / K_R \tag{A 8}$$

is obtained. Equations (A 4)–(A 8) then yield:

$$k_{on} \approx k_{diff} c_H \left(1 + \frac{c_{OH}}{K_R} + \frac{c_P}{K_R + K_P}\right) \tag{A 9}$$

At neutral pH ($c_H \approx c_{OH} \approx 10^{-7}$ M) and for $c_P \gg c_{OH}$ and $K_P \lesssim K_R \approx 10^{-7}$ M, the protonation rate constant k_{on} is largely dominated by the last term in (A 9) describing protonation by the buffer acid HP:

$$k_{on} \approx k_{diff} \frac{c_H c_P}{K_R + K_P} = \frac{k_{diff} c_{HP}}{1 + K_R/K_P}. \tag{A 10}$$

With $k_{diff} \approx 10^{10}$ M^{-1} s^{-1} (Eigen 1963), $c_{HP} \approx 10^{-4}$ M, and $K_R \approx K_P$, k_{on} becomes of the order of 10^6 s^{-1}, much larger than the estimated proton translocation rate of $10^3 - 10^4$ s^{-1} through a stator element.

In an analogous way, one obtains for the overall rate k_{off} of deprotonation of HR:

$$k_{off} = k_{-1}\left(1 + \frac{c_{OH}}{K_R} + \frac{c_P}{K_R + K_P}\right) \approx \frac{k_{-1} c_P}{K_R + K_P}. \tag{A 11}$$

With $K_R \approx K_P \approx 10^{-7}$ M, $k_{-1} \approx k_{diff} K_R \approx 10^3$ s^{-1}, and $c_P \approx 10^{-4}$ M, k_{off} becomes of the order of 10^6 s^{-1}.

Appendix B

Derivation of (17) and (18)

We consider the reaction cycle of Fig. 4 under the condition of vanishing driving forces ($\psi' = \psi''$, $c' = c''$, $M_e = 0$). In this case, according to the principle of detailed balance, every single reaction step is in equilibrium separately:

$$\frac{x[A_{j+1}]}{x[A_j]} = \frac{\tilde{k}'_j}{\tilde{k}''_{j+1}} \qquad (j = 0, 1, 2, \ldots, n) \tag{B 1}$$

$$\frac{x[B_{j+1}]}{x[B_j]} = \frac{\tilde{l}'_j}{\tilde{l}''_{j+1}} \tag{B 2}$$

Using the identity

$$\frac{x[A_1]}{x[A_0]} \cdot \frac{x[A_2]}{x[A_1]} \cdots \frac{x[A_{n+1}]}{x[A_n]} \equiv \frac{x[A_{n+1}]}{x[A_0]} \tag{B 3}$$

and inserting (6) and (B 1) yields (17). In a similar way, the identity

$$\frac{x[B_1]}{x[B_0]} \cdot \frac{x[B_2]}{x[B_1]} \cdots \frac{x[B_{n+1}]}{x[B_n]} \equiv \frac{x[B_{n+1}]}{x[B_0]} \tag{B 4}$$

together with (5), (6) and (B 2) yields (18).

References

Belyakova TN, Glagolev AN, Skulachev VP (1976) Electrochemical gradient of H^+ ions as a direct source of energy during bacterial locomotion. Biokhimiya 41:1206–1210

Berg HC (1974) Dynamic properties of bacterial flagellar motors. Nature (Lond) 249:77–79

Berg HC (1975) Chemotaxis in bacteria. Annu Rev Biophys Bioeng 4:119–136

Berg HC (1983) Random walks in biology. Princeton University Press, Princeton, NJ, pp 1–142

Berg HC, Khan S (1983) A model for the flagellar motor. In: Sund H, Veeger C (ed) Motility and recognition in cell biology. De Gruyter, Berlin, pp 486–497

Berg HC, Turner L (1979) Movement of microorganisms in viscous environments. Nature (Lond) 278:349–351

Berg HC, Manson MD, Conley MP (1982) Dynamics and energetics of flagellar rotation in bacteria. Proc Symp Soc Exp Biol 35:1–31

Blair DF, Berg HC (1988) Restoration of torque in defective flagellar motors. Science 242:1678–1681

Block SM, Berg HC (1984) Successive incorporation of force-generating units in the bacterial rotary motor. Nature (Lond) 309:470–472

Block SM, Blair DF, Berg HC (1989) Compliance of bacterial flagella measured with optical tweezers. Nature 338:514–517

Coulton JW, Murray RGE (1978) Cell envelope associations of Aquaspirillum serpens flagella. J Bacteriol 136:1037–1049

Cox DR, Miller HD (1977) The theory of stochastic processes. Chapman and Hall, London, p 398

De Pamphilis ML, Adler J (1971) Fine structure and isolation of the hook-basal boday complex of flagella from *Escherichia coli* and *Bacillus subtilis*. J Bacteriol 105:384–395

Eigen M (1963) Proton transfer, acid-base catalysis and enzymatic hydrolysis. Part I: Elementary processes. Angew Chem (Intern edn) 3:1–19

Glagolev AN, Skulachev VP (1978) The proton pump is a molecular engine of motile bacteria. Nature (Lond) 272:280–282

Hille B (1984) Ionic channels of excitable membranes. Sinauer Associates, Sunderland, p 426
Khan S (1988) Analysis of bacterial flagellar motion. Cell Motil Cytoscel 10:38–46
Khan S, Berg HC (1983) Isotope and thermal effects in chemiosmotic coupling to the flagellar motor of Streptococcus. Cell 32:913–919
Khan S, Macnab RM (1980) Proton chemical potential, proton electrical potential and bacterial motility. J Mol Biol 138:599–614
Khan S, Meister M, Berg HC (1985) Constraints on flagellar rotation. J Mol Biol 184:645–656
Khan S, Dapice M, Reese TS (1988) Effects of mot gene expression on the structure of the flagellar motor. J Mol Biol 202:575–584
Kirkpatrick S, Stoll EP (1981) A very fast shift-register sequence random number generator. J Comput Phys 40:517–526
Kobayashi S (1988) Diffusion motor as a model of flagellar motor of bacteria. Ferroelectrics 88:335–346
Krulwich TA (1986) Bioenergetics of alkalophilic bacteria. J Membr Biol 89:113–125
Läuger P (1977) Ion transport and rotation of bacterial flagella. Nature (Lond) 268:360–362
Läuger P (1988) Torque and rotation rate of the bacterial flagellar motor. Biophys J 53:53–65
Lowe G, Meister M, Berg HC (1987) Rapid rotation of flagellar bundles in swimming bacteria. Nature (Lond) 325:637–640
Macnab RM (1978) Bacterial motility and chemotaxis: the molecular biology of a behavioural system. CRC Crit Rev Biochem 5:291–341
Macnab RM (1979) How do flagella propell bacteria? Trends Biochem Sci 4:N10–N13
Macnab RM (1980) Sensing the environment. Bacterial chemotaxis. In: Goldberger RF (ed) Biological regulation and development, vol 2. Plenum Press, New York, pp 377–412
Macnab RM (1987) Motility and chemotaxis. In: Neidhardt FD (ed) *Escherichia coli* and *Salmonella typhimurium*: cellular and molecular biology. American Society for Microbiology, Washington, DC, pp 70–83
Macnab RM, Aaizawa SI (1984) Bacterial motility and the bacterial flagellar motor. Annu Rev Biophys Bioeng 13:51–83
Manson MD, Tedesco P, Berg HC, Harold FM, van der Drift C (1977) A protonmotive force drives bacterial flagella. Proc Natl Acad Sci USA 74:3060–3064
Manson MD, Tedesco PM, Berg HC (1980) Energetics of flagellar rotation in bacteria. J Mol Biol 138:541–561
Matsuura S, Shioi J-I, Imae Y (1977) Motility in Bacillus subtilis driven by an artificial protonmotive force. FEBS Lett 82:187–190
Meister M, Lowe G, Berg HC (1987) The proton flux through the bacterial flagellar motor. Cell 49:643–650
Meister M, Caplan SR, Berg HC (1989) Dynamics of tightly-coupled mechanism for flagellar rotation. Biophys J 55:905–914
Mitchell P, Moyle J (1974) The mechanism of proton translocation in reversible proton-translocating adenosine triphosphatases. Biochem Soc (Spec Publ) 4:91–111
Murata T, Yano M, Shimizu H (1989) A model of bacterial flagellar motor: Free energy transduction and self-organization of rotational motion. J Theor Biol 139:531–559
Oosawa F, Hayashi S (1983) Coupling between flagellar motor rotation and proton flux in bacteria. J Phys Soc Jpn 52:4019–4028
Oosawa F, Masai J (1982) Mechanism of flagellar motor rotation in bacteria. J Phys Soc Jpn 51:631–641
Prod'hom B, Pietrobon D, Hess P (1987) Direct measurement of proton transfer rates to a group controlling the dihydropyridin-sensitive Ca^{2+} channel. Nature 329:243–246
Ravid S, Eisenbach M (1984) Direction of flagellar rotation in bacterial cell envelopes. J Bacteriol 158:222–230
Ridgeway HF, Silverman M, Simon MI (1977) Localization of proteins controlling motility and chemotaxis in *Escherichia coli*. J Bacteriol 132:657–665
Schuster P (1987) Hydrogen bonds. In: Meyers RA (ed) Encylopedia of physical science and technology, vol 6. Academic Pess, New York, pp 518–554
Shioi J-I, Matsuura S, Imae Y (1980) Quantitative measurements of protonmotive force and motility in Bacillus subtilis. J Bacteriol 144:891–897
Silverman M (1980) Building bacterial flagella. Q Rev Biol 55:395–408
Silverman M, Simon M (1977) Bacterial flagella. Annu Rev Microbiol 31:397–419
Stewart RC, Dahlquist FW (1987) Molecular components of bacterial chemotaxis. Chem Rev 87:997–1025
Zwolinsky BI, Eyring H, Reese CE (1949) Diffusion and membrane permeability. J Phys Chem 53:1426–1453